ORIGINAL ARTICLE

Hemocyte activation and nodule formation in the giant keyhole limpet, *Megathura crenulata*

Gary G. Martin[1] | Stephanie Stamnes[1] | Nicola Henderson[1] | Juliette Lum[1] | Nicole Rubin[2] | Jonathan P. Williams[1,3]

[1]Department of Biology, Occidental College, Los Angeles, California, USA

[2]Bio-Rad, Hercules, California, USA

[3]Vantuna Research Group, Occidental College, Los Angeles, California, USA

Correspondence
Gary G. Martin, Department of Biology, Occidental College, Los Angeles, CA 90041, USA.
Email: gmartin@oxy.edu

Abstract

The giant keyhole limpet, *Megathura crenulata*, lives in rocky intertidal and subtidal environments along the Southern California coast, where it is exposed to viruses, bacteria, and other potential pathogens. We demonstrate that when exposed to bacteria or latex beads, hemocytes from specimens of *M. crenulata in vivo* and *in vitro* immediately become adhesive and form nodules. The rapid activation of hemocytes suggests a role for an array of recognition proteins, and inhibition of nodulation by the tripeptide Arg–Gly–Asp indicates that integrins are involved. The morphological changes involved with nodule formation include the rapid extension of lamellipodia, phagocytosis of particles, and compaction of the hemocyte aggregates. The number of nonadherent hemocytes rapidly decreases as aggregates form. The elimination of bacteria is due to a dynamic hemocyte response, rather than antibacterial factors in the plasma. These findings are compared to work on other gastropods and expand the current knowledge on the immune response of molluscs, such as *M. crenulata*, which is increasing in importance as they continue to be raised in aquaculture for pharmacological use.

KEYWORDS
archeogastropoda, gastropod, innate immunity, Mollusca

1 | INTRODUCTION

Molluscs lack an adaptive immune system and rely on innate immunity to deal with foreign particles and pathogens that have penetrated surface barriers such as shells and mucous coatings (Gliński & Jarosz, 1997; Loker, 2010; Martin et al., 2018). Infection by bacteria and other pathogens induces a rapid immune response comprising both cellular and humoral factors, but a body must first be recognized as foreign in order to initiate a response. This may involve interactions with plasma factors such as phenoloxidase (Coles & Pipe, 1994; Luna-González et al., 2003), and antimicrobial compounds such as lysozyme (Cheng & Gerhart, 1978). Foreign particles may also bind to hemocytes via lectins (Humphries & Yoshino, 2003), integrins (Davids & Yoshino, 1998), toll-like receptors (Loker et al., 2004), pattern-recognition motifs bound to cell membranes, or a variety of other suggested receptors (Chen & Bayne, 1995). Once the body is established as foreign, signaling molecules such as cytokines (Koutsogiannaki & Kaloyianni, 2010) trigger intracellular processes that activate hemocytes to adhere to foreign materials and to one another to form nodules. Reorganization of the cytoskeleton allows for phagocytosis of small particles (Canesi et al., 2002), and nodule formation allows for sequestration of many particles or encapsulation of large objects such as multicellular parasites (Canesi et al., 2002; Robohm, 1984; Sminia et al., 1974; Yousif et al., 1980). Fixed phagocytes, which have been described from the connective tissue and the site of infection of some species (Matricon-Gondran & Letocart, 1999; Ottaviani & Cossarizza, 1990; Sminia, 1972), also contribute to defense against microbes.

The role of molluscan hemocytes is not only limited to the immune response but also includes functions such as wound repair,

shell deposition, and excretion (Cheng, 1981; Franchini & Ottaviani, 2000; Hanington et al., 2010). Understanding hemocyte function requires the identification of different types of hemocytes, and several classification schemes have been proposed. Several schemes identify two or three morphologically distinct types of circulating cells (Accorsi et al., 2013; Cueto et al., 2015; Pengsakul et al., 2013; Voltzow, 1994), with one type containing obvious granules. However, some species lack granulocytes. Two morphologically distinct types of agranular hemocytes have been identified in the molluscs *Pomacea canaliculata* (LAMARCK 1822), *Haliotis tuberculata* LINNAEUS 1758, and *Planorbarius corneus* (LINNAEUS 1758); the larger type of agranular hemocyte is capable of phagocytosing bacteria (Accorsi et al., 2013; Ottaviani et al., 1992). By contrast, *Lymnaea stagnalis* (LINNAEUS 1758) (Sminia, 1972; Sminia et al., 1974), *Biomphalaria glabrata* (SAY 1818) (Dikkeboom et al., 1985; Matricon-Gondran & Letocart, 1999), *Aplysia californica* J. G. COOPER 1863, and *Megathura crenulata* (G. B. SOWERBY I 1825) (Martin et al., 2007; Travers et al., 2008) appear to have only one type of hemocyte, which may display different morphologies depending on cell maturation. This great variation among species makes it currently impossible to present a unified classification scheme based on the morphology of hemocytes in Mollusca.

Knowledge of hemocyte structure and function is increasing, as well as our appreciation for the arsenal of molecules and processes involved in the immune response. The interplay of these aspects of the innate immune response within molluscs requires further attention. Pauley et al. (1971) and Pauley and Krassner (1972) presented some of the first observations of in vivo whole body responses to the challenge of particles injected into the hemocoel of the gastropod *A. californica*. Injections of India ink particles or carmine dye resulted in loose nodule formation and phagocytosis by individual hemocytes. Most aggregates were found near the site of injection, with little accumulation in the gills or other organs. Bacteria injected into the blood were cleared within 8 h, corresponding with a drop in the total number of circulating hemocytes, which recovered within 24 h. In 1974, Bayne's experiments on the pulmonate *Helix pomatia* LINNAEUS 1758 determined that the snail could survive clearance of one trillion bacteria from its hemolymph. Neither hemocyte phagocytosis nor bacteria lysis was involved, and clearance probably involved fixed phagocytes and aggregations of circulating hemocytes especially within the digestive gland. Studies on the freshwater pulmonate *L. stagnalis* demonstrated that 99% of bacteria injected into the snail's hemolymph were cleared within 2 h (van der Knaap et al., 1981). Bacteria were phagocytosed and degraded by fixed phagocytes and circulating hemocytes, which declined rapidly following injections. More recently, Cueto et al. (2013) and Cueto et al. (2015) have described nodules being formed in circulation and in the vasculature of the kidney in *P. canaliculata* in response to experimental bacterial infections. This work is supported by Rodriguez et al. (2018), who proposed that some organs, such as the kidney and lung in *P. canaliculata*, may facilitate hemocyte–antigen interactions in ways analogous to lymph nodes in vertebrates. In a taxon as large and diverse as the Gastropoda, it is not surprising that a variety of responses (phagocytosis, nodule formation, organ-specific clearance, and fixed phagocytes) may be involved or that clearance mechanisms have been investigated in only a few species. This study aims to expand our knowledge regarding removal of foreign material from circulation by hemocyte nodulation in *M. crenulata*.

The giant keyhole limpet, *M. crenulata*, lives in rocky coastal environments along the Southern California coast (Morris et al., 1980), where it faces the challenge of exposure to microbial pathogens and environmental pollutants known to affect molluscan immune responses (Giron-Perez, 2010; Gopalakrishnan et al., 2009). The limpet is unusual in that most of its external surface, including the shell, is covered by a glycocalyx-coated epithelium (Martin et al., 2018). *M. crenulata* is a model for investigating the molluscan immune response. Studies of *M. crenulata* are of increasing importance because it is raised in aquaculture for pharmacological use as the sole provider of keyhole limpet hemocyanin (KLH). KLH is an immune-stimulating molecule used in active immunotherapies, and it is a key component of several cancer drugs currently undergoing clinical trials (Fenstermaker et al., 2016; Miles et al., 2011; Pyzer et al., 2014). This article compares (1) the time sequence of nodule formation, (2) the efficiencies of particle removal from circulation by circulating hemocytes, and (3) the morphological changes to hemocytes during nodule formation in both in vivo and in vitro experiments.

2 | METHODS

2.1 | Limpet care and bacteria culture

Giant keyhole limpets, *M. crenulata*, were collected in 2017–2019 from southern California rocky reefs along the Palos Verdes peninsula by SCUBA divers in the Vantuna Research Group at Occidental College under California Department of Fish and Wildlife Scientific Collecting Permit # SC-007227. Limpets were maintained in seawater aquaria (16°C, salinity 33 ppt). No food items were added; however, limpets consumed bacteria, protists, and algal films on aquaria walls, as evidenced by radulation tracks. Only healthy limpets were used, based on intact epithelia, strong adherence to aquaria walls, and total hemocyte counts within an expected range of $2–9 \times 10^6$ cells/ml. Live cultures of *Vibrio fischeri* were purchased from Ward Scientific (#470176-340) and grown at 23°C on plates of tryptic soy agar (TSA; Difco 236950) with added 5% NaCl (TSA + NaCl). Colonies were scraped from plates and mixed with phosphate buffered saline with additional NaCl to a final concentration of 3% NaCl (PBS + NaCl), and concentrations were determined with a spectrophotometer; an 80% transmittance at 600 nm was equivalent to a concentration of 10^8 bacteria/ml (Mikulski et al., 2000). Bacteria were diluted to desired concentrations in sterile PBS + NaCl.

2.2 | In vitro tests for bacterial clearance and hemocyte viability

When removed from a limpet, hemolymph does not clot and form a gel, but the contained hemocytes aggregate quickly. To observe in vitro nodule formation and its effect on the concentration of bacteria in suspensions, the following experiments were performed on 10 limpets, using 2 limpets for each of the following times: 5, 15, 30, 60, and 180 min. From each limpet, 45 ml of hemolymph containing an average of 4×10^6 hemocytes/ml was collected by cannulization of the buccal sinus of individual limpets, following the method described in US patent # 6,852,338 B2. Each sample was mixed with 5 ml of culture of *V. fischeri* (Ward's Science 470176-340) at 5×10^6 bacteria/ml in PBS + NaCl. Aliquots (10 ml) were added to five 35-mm-diameter plastic petri dishes (Fisher Scientific FB0875713A) and placed on a rotating rocker set to 16 RPM at 23°C to ensure continuous mixing and allow for observations on nodule formation. The two sets of dishes, produced from the 10 limpets, were used in the following manner after mixing for 5, 15, 30, 60, or 180 min. One dish at each time was used for two tests and the second dish was used for morphological examination of the nodules (see below). The first test quantified the bacteria remaining in suspension; small aliquots (10 μl) of solution were collected at each time point and cultured on plates of TSA + NaCl. After 48 h at 23°C, colony-forming units were counted. Aliquots of pure blood and bacteria in PBS + NaCl were cultured on TSA + NaCl plates to test for contaminated blood and to assess bacterial dilutions, respectively. Percent bacterial clearance over time was calculated by dividing bacteria concentration at each time point by the initial concentration.

For the second test, one dish at each time point described above was used to quantify the viability of hemocytes using the trypan blue exclusion test, as described by Stober (2015). Petri dishes were rinsed with PBS + NaCl and then 5 ml of a 0.2% solution of trypan blue in PBS + NaCl was added. After 3 min, 200 hemocytes were observed and the number of blue-stained (dead) cells was expressed as percentage of the total cells. Individual hemocytes as well as cells in small nodules (<10 hemocytes) were readily assessed yet made up a tiny percentage of the total number of hemocytes. Live versus dead cells in larger aggregates could not be quantified because the thickness of the nodules prevented the discrimination of the two cell types by examination under light microscopy.

2.3 | Test for antibacterial factors

To determine whether the loss of bacteria from culture suspension was due to antibacterial factors, blood was collected from five limpets and tested separately. Blood was passed through a syringe filter (Fisherbrand 09-719A with 0.22-μm pore size) to produce a cell-free plasma. Cultures of *V. fischeri* suspended in PBS + NaCl (0.3 ml) were mixed with either 2.7 ml of filtered (i.e., cell-free) plasma or PBS + NaCl (control) to achieve a final concentration of 10^4 bacteria/ml. Filtered hemolymph was cultured to test for bacterial contamination. After incubations for 30 min, 1 h, and 2 h, blood was diluted tenfold for four dilutions, and 100 μl of each dilution was spread on two TSA + NaCl plates for each time point. Cultures were incubated for 2 days at 23°C, and the plates with a quantifiable density of colony-forming units

were analyzed, whereas plates with <10 colonies or colonies too numerous to count were discarded. The experiment was performed in duplicate.

2.4 | Morphology of nodules formed in vitro

The second set of dishes produced as described in the above experiments were processed for morphological analysis. At each of the time points between 5 and 180 min, nodules formed in the presence of bacteria were collected and processed for examination by light microscopy (LM), and scanning and transmission electron microscopy (SEM and TEM, respectively). Two additional sets of nodules were produced at each time point. In one, 1-μm-diameter latex beads (carboxylate-modified polystyrene Sigma L4655) at a concentration of 10^6 beads/ml blood were substituted for the bacteria. Their spherical shape made them easier to identify in SEM images, in which elongate bacteria could be confused with filopodia. In the third variation, neither bacteria nor beads were added and PBS + NaCl alone served as a control. Five limpets were used in each experiment. Each dish was initially photographed with a light microscope at each time point, and the percent area covered by adhered nodules was quantified using Image J software.

Nodules from each treatment and each time point were collected for processing and examination by LM, SEM, and TEM. Samples were rinsed in PBS + NaCl and fixed overnight in 3% glutaraldehyde in 0.1 M sodium cacodylate buffer (pH 7.6). All samples were washed in buffer and post-fixed 1 h in 1% OsO_4 in 0.1 M sodium cacodylate buffer. For LM and TEM, samples were stained en bloc in 3% uranyl acetate in 0.1 M sodium acetate buffer for 1 h, dehydrated through a graded series of ethanol, and infiltrated and embedded in plastic (Spurr, 1969). Thick (0.5 μm) and thin (90 nm) sections were cut, stained with methylene blue or lead citrate, and viewed by LM or TEM (Zeiss EM 109), respectively. Samples for SEM were dehydrated, soaked in hexamethyldisilazane (HMSD, Pella 18605) for 15 min, air-dried, mounted on stubs, coated with gold in a Technics Hummer VI Sputter Coater, and examined in a Phenom SEM.

To determine whether hemocyte adhesion and nodule formation was inhibited by the tripeptide Arg-Gly-Asp (RGD), an amino acid sequence recognized by integrins, 3 ml of blood from five separate limpets was mixed immediately with RGD (Sigma A8052) for a final concentration of 10-mM RGD. An equal volume of hemolymph from each limpet was not mixed with RGD and served as controls. Dishes were placed on a rocker for the same times listed above and then the preparations were fixed by the addition of 1-ml glutaraldehyde fixative and processed as described above for examination using a dissecting microscope and SEM.

2.5 | Bacterial clearance in vivo

To compare bacterial clearance in vivo with values obtained with in vitro experiments, bacteria were injected into the hemolymph of limpets and their concentrations quantified at times after injection. First, it was necessary to determine the volume of blood in limpets of various weights so that the concentration of bacteria injected into a limpet would result in each limpet receiving a similar concentration of bacteria. Fourteen limpets ranging 100–500 g in mass were used for an estimation of their blood volume. Data were collected from limpets used in this study and in two previous studies on the morphology of the gut and skin (Martin et al., 2010; Martin et al., 2018). Each limpet was sliced in half to separate the foot from the dorsal half containing the shell, mantle, and viscera. These tissues were further sliced to facilitate blood loss, and hung above collection tubes in a cold room at 4°C. After 4 h, the fluid collected from these organs and the hemolymph released during the initial dissection were pooled to provide an approximate estimation of total body hemolymph volume, which is in the range reported in other molluscs (see Martin et al., 1958).

Bacteria diluted in 1 ml of PBS + NaCl were injected into the sub-buccal cavity of six limpets with a needle (BD 305167 21G × 1.5″) to yield a final concentration of 10^4 bacteria/ml of hemolymph in each limpet. Prior to injection, a drop of hemolymph (∼100 μl) was collected using a needle, and additional samples were collected at 1-, 4-, 8-, 24-, and 48-h post-injection. At each time point, a total hemocyte count (THC) was determined using a hemocytometer, and 10 μl of blood was cultured on plates of TSA + NaCl to quantify bacteria in the blood. Following incubation at 23°C for 48 h, colony-forming units were counted. Pure hemolymph (10 μl) and 10 μl of bacteria diluted in PBS + NaCl were plated as controls. Duplicate plates were cultured and counted for each time point.

To determine whether the injection alone affected the THC, six limpets were injected with an appropriate volume of PBS + NaCl, and another six were merely punctured with a needle to obtain ∼10 μl of blood for a THC with no fluid injected. Blood samples were collected for THC counts and cultured at each of the times tested above.

2.6 | Morphology of nodules binding to tissues in vivo

The following procedure was developed to determine whether nodules formed following the injection of bacteria into living limpets could be observed binding to tissues lining the circulatory system, similar to nodules binding to the petri dish in the in vitro experiments. Cultures of *V. fischeri* were injected into the sub-buccal sinus of two limpets to produce a concentration of 10^4/ml for the entire body. The needle was glued into position with commercial cyanoacrylate glue so that the tip of the needle would stay in place and could be located during subsequent dissection. After 30 min, blood was drained as described for total blood volume estimations and a 1 × 1-cm piece of the ventral surface of the buccal mass, posterior to the site of injection, was

rinsed in PBS + NaCl, processed, and examined by SEM. As a control, the same organs were examined in two limpets that had not been injected with bacteria, and merely bled quickly as described for total blood volume values, and samples of the ventral buccal mass were processed for examination by SEM.

2.7 | Statistics

All data analyses were performed using R version 4.1.0 (R Core Team, 2021). The relationship between limpet body weight and blood volume was modeled by linear regression using the lm function. In vitro and in vivo bacterial clearance data were each fit separately using nonlinear least squares to an asymptotic regression model using the nls and SSasymp functions, and to an exponential decay model using nls and the NLS.expoDecay function in the aomisc package (Onofri, 2020). To determine which model best fit each set of bacterial clearance data, model parameters were constructed and ranked according to second-order Akaike Information Criterion (AICc, AIC for small samples). Model parameters were constructed using the AICc function in the MuMIn package (Bartoń, 2020), and Akaike weights (w_i) were calculated to assess the relative likelihood of each model. Akaike weights were interpreted as the weight of evidence in favor of each model (Akaike, 1973; Burnham & Anderson, 2002). For visualization, 95% confidence intervals for the selected models were calculated using the predFit function in the investr package (Greenwell & Schubert Kabban, 2014).

Mixed-model ANOVAs were calculated using the lme function from the nlme package (Pinheiro et al., 2021) to determine whether there was an overall difference over time in: (1) in vitro bacterial clearance, (2) in vivo bacterial clearance, (3) antibacterial properties between blood plasma and a control, (4) in vitro nodule formation between treatments, and (5) hemocyte count between treatments. Pairwise differences between each sampling time or variable were calculated using the emmeans function from the emmeans package (Lenth, 2021), and *p* values were adjusted using the Tukey method. For visualization, means and 95% confidence intervals were calculated by bootstrapping (1000 permutations).

3 | RESULTS

3.1 | In vitro tests for bacterial clearance and hemocyte viability

The clearance of the cultures of *V. fischeri* from limpet hemolymph in the in vitro tests was followed by mixing blood with bacteria in petri dishes on rockers as described above. The abundance of free bacteria in suspension significantly decreased over time ($F_{[5,45]} = 308.2$, $p < .001$) following an asymptotic regression model ($w_i = 1$) and decreased significantly at every observation time ($p < .001$ for all contrasts; Figure 1A). The ratio of hemocytes to bacteria was ∼36:1, and 80% of bacteria were cleared within 3 h.
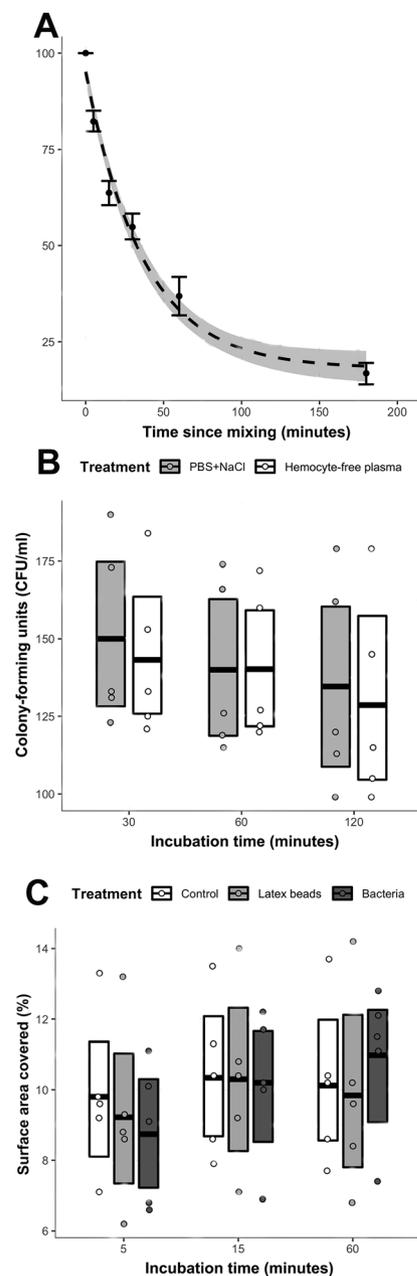
FIGURE 1 In vitro experiments in hemocyte activation and nodule formation in *Megathura crenulata*. **A.** Removal of bacteria (*Vibrio fischeri*) from cultures of hemocytes monitored over 3 h ($n = 10$). Error bars represent bootstrapped 95% confidence intervals (1000 permutations). Gray ribbon represents 95% confidence intervals of the asymptotic regression model. **B.** Colony-forming units of *V. fischeri* cultured after 30, 60, and 120 min of incubation in hemocyte-free plasma; there was no significant difference in the number of colonies formed between treatments, suggesting that antimicrobial factors in the plasma were absent. Incubations in PBS + NaCl served as controls. Boxes represent means and bootstrapped 95% confidence intervals (1000 permutations); $n = 5$ per treatment. **C.** Percentage of the total surface area of the petri dish covered by nodules after 5, 15, and 60 min of incubation with pure plasma (control), latex beads, and bacteria; there were no significant differences between treatments. Boxes represent means and bootstrapped 95% confidence intervals (1000 permutations); $n = 5$ per treatment

The viability of hemocytes was examined after 1, 4, 8, 24, and 48 h of culture. At 1 and 4 h, an average of 0.05% ($SD = 0.02$%) of the hemocytes took up the trypan blue dye. That percentage rose to an average of 0.4% ($SD = 0.02$%) by 24 h and an average of 0.7% ($SD = 0.03$%) at 48 h of culture, indicating little cell death occurred at all times examined. These estimates are based on counts of individual cells and small (<10 cell) nodules; the presence or absence of staining of hemocytes within larger nodules could not be determined microscopically because of their opacity. No individual cells remained in suspension; all settled onto the petri dishes. Only a tiny number (<2%) of nodules did not settle onto the petri dish surface, and these were typically too large to accurately count hemocytes.

3.2 | Test for antibacterial factors

The significant decline ($F_{[2,16]} = 11.1$, $p = .001$) in the number of cells of *V. fischeri* from culture supernatant was not due to their destruction or elimination by serum factors. No statistical difference in the number of bacteria, as determined by CFU counts (Figure 1B), was observed between bacteria incubated in plasma and those in PBS + NaCl (control) when assessed after 30, 60, and 120 min of culture ($F_{[1,8]} = 0.05$, $p = .823$), and there was no interaction between time and treatment ($F_{[2,16]} = 0.72$, $p = .501$).

3.3 | Morphology of nodules formed in vitro

The addition of blood from limpets to plastic petri dishes, with or without the addition of bacteria or latex beads, caused hemocytes to rapidly become adhesive, extend filopodia and lamellipodia, bind to adjacent hemocytes and particles still in suspension, and settle and attach to petri dishes. The process appeared the same whether the hemocytes were exposed to bacteria, beads, or merely the plastic syringes and petri dishes, so the following descriptions refer to all treatments. Most individual cells and nodules settle and bind to the petri dish within 5 min, covering ∼10% of the bottom of the dish. There was a significant increase in the percent coverage during the next 60 min of incubation across all treatments ($F_{[2,24]} = 8.38$, $p = .002$), but no significant difference between treatments ($F_{[2,12]} = 0.02$, $p = .918$) or interaction between time and treatments ($F_{[4,24]} = 2.20$, $p = .100$) (Figure 1C). Within 15 min from the start of incubation, individual hemocytes and 85% of nodules had settled and attached to the petri dish (Figure 2A). Nodules bound to the petri dish, as well as the few remaining in suspension, were mostly formed by 15 min of incubation, and any further enlargement was only achieved by additional hemocytes settling out of suspension onto other nodules (Figure 2B). Nodules attached to the dish did not migrate.

When examined after 15 min of culture, individual hemocytes settling onto the petri dish rapidly flattened and extended lamellipodia primarily around their margins. Hemocytes settling onto the surface of newly formed nodules (in suspension and attached) had a similar morphology in all treatments (controls, mixed with bacteria or beads);
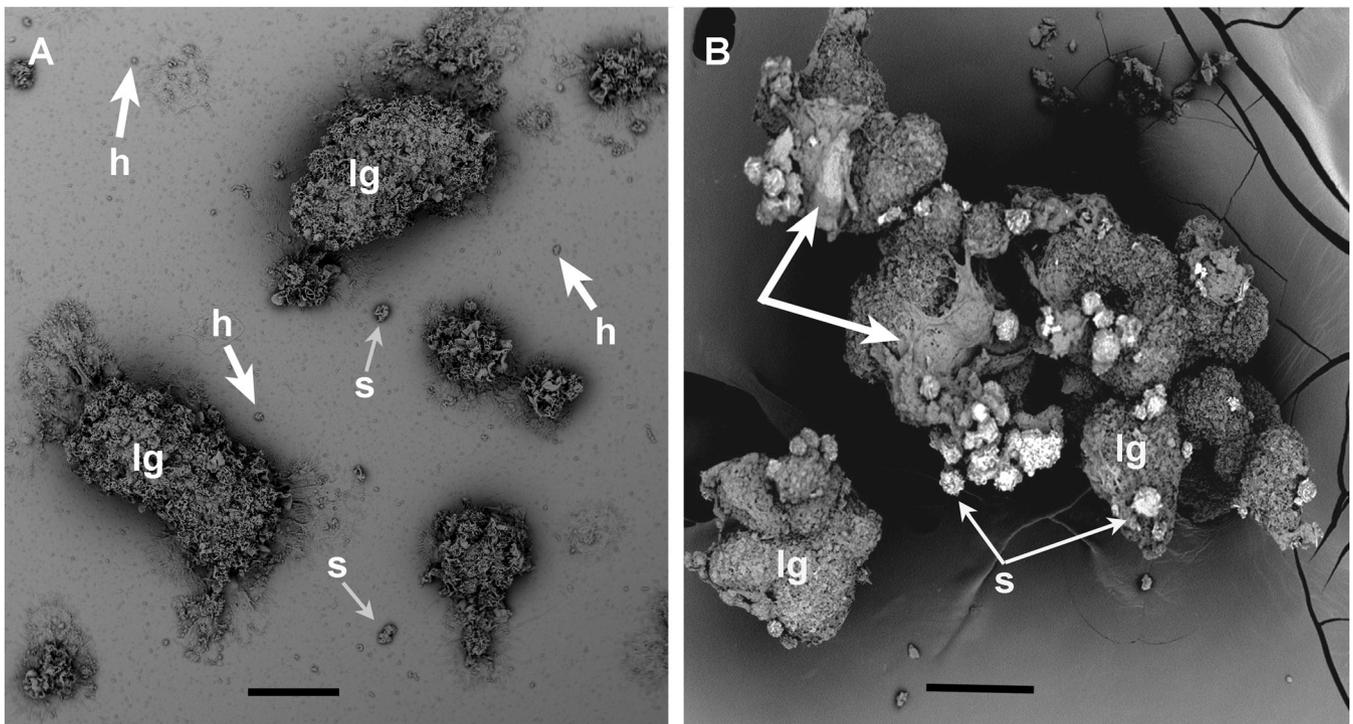
FIGURE 2   Scanning electron micrographs of in vitro formation of nodules by hemocytes in *Megathura crenulata*. **A.** Scanning electron micrograph showing variation in size of nodules adhering to petri dish after 30 min; nodules ranged in size, from small (<10 hemocytes) to large, or were just individual hemocytes. All hemocytes produced cytoplasmic extensions, seen in higher magnification images (Figure 3A,B). **B**. SEM of nodules that remained in suspension after 30 min of incubation. Note how smaller nodules bind and merge into the larger masses. Two areas (unlabeled arrows) are covered by material presumed to be precipitated plasma proteins. Scale bars: A = 50 µm; B = 100 µm. h, individual hemocyte; lg, large nodule; s, small nodule

they were spherical and extended sheet-like lamellipodia with finger-like filopodia (Figure 3A,B). By 1 h, cells forming the outer layer of nodules were flat with very few extensions (Figure 3C,D). After 15 min, spaces were common between hemocytes (Figure 3E) and formed the bulk of each nodule. By 4 h, the nodule mass was compact (Figure 3F), with few spaces between cells, and nodule morphology was relatively unchanged after this time up until 48 h, the last time we examined. When hemolymph was mixed with RGD and examined at the same time points as described above, nodules did not form; individual cells settled onto the petri dish, remained ovoid, and had small, ovoid blebs on their surface, but no filopodia or lamellipodia (Figure 3G).

The process of phagocytosis of bacteria and beads by hemocytes was examined by LM and TEM. No differences were observed between nodules that remained in suspension and those attached to the substrate, nor between treatments with different particles. Hemocytes recently attached to a nodule typically had bacteria bound to their apical surface and cytoplasmic extensions surrounding the bacteria (Figure 4A). The nucleus in these hemocytes was ovoid, with heterochromatin forming patches within the nucleus as well as lining the nuclear envelope, and there were few signs of nuclear pores (Figure 4A). Electron-lucent vesicles, 0.15-µm diameter, often in close association with Golgi bodies, and

electron-dense mitochondria were common. In later stages, after incubation with latex beads, beads could be seen bound by hemocytes along the nodule surface and within phagocytic vacuoles (Figure 4B). The beads, especially those on the surface, appeared with moderately electron-dense material that had collapsed, presumably due to processing, as previously described (Giulianini et al., 2003). Bacteria and latex beads, respectively, could be seen within hemocytes that were deeper into nodules at the 30-min time point (Figure 4C,D). The hemocytes were densely packed, with no interstitial spaces, and bacterial debris appeared as heterogeneous material of intermediate electron density in vacuoles. Vacuoles were also observed in control nodules, which formed without the addition of bacteria or beads. Examination of the surface of phagocytosed beads showed a thin (60 nm) layer of moderately electron-dense material (Figure 4E) along with tiny cylinders (∼40-nm diameter), which were also observed on beads in plasma outside developing nodules (Figure 4F).

3.4 | Bacterial clearance in vivo

Figure 5A shows the relationship between limpet body weight and blood volume. Note that blood volume was ∼45% of total body
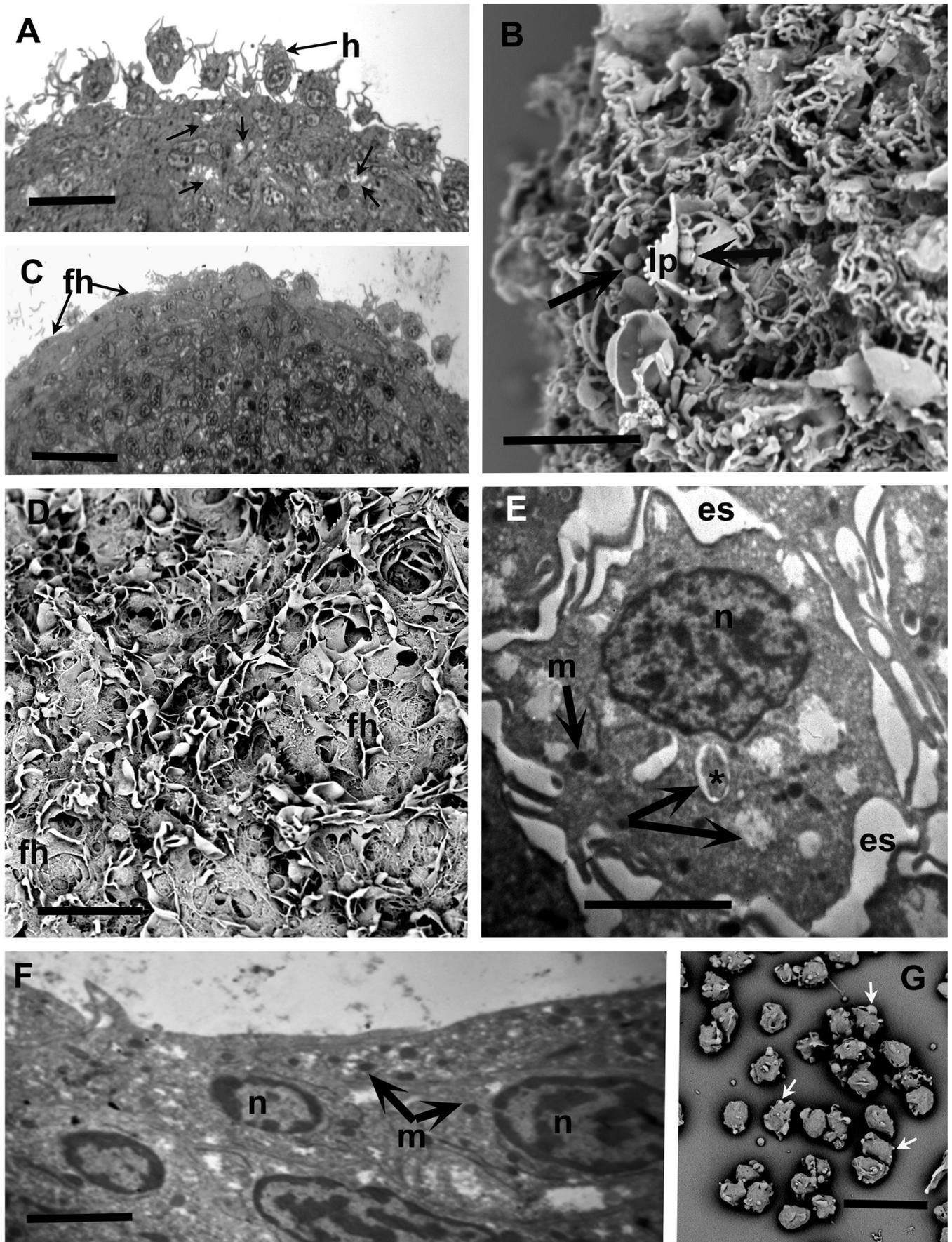
FIGURE 3   Legend on next page.

FIGURE 3 Light, scanning electron, and transmission electron micrographs of nodules formed by hemocytes in *Megathura crenulata*. **A.** Light micrograph of a section through a nodule formed after 15 min, showing spherical hemocytes displaying numerous cytoplasmic extensions binding to the surface of the enlarging nodule. Arrows point to extracellular spaces. **B.** SEM of surface of nodule incubated for 15 min with latex beads. The outline of individual hemocytes is obscured by the extensive cytoplasmic extensions. Arrows point to three latex beads on either side of a lamellipodium. **C.** Light micrograph of a section through a nodule incubated for 1 h with bacteria. Note that the surface of the nodule is smoother, with flattened hemocytes showing reduced cytoplasmic extensions. Extracellular spaces are not seen. **D.** SEM of the surface of a nodule formed after 1-h incubation, showing many flattened hemocytes with greatly reduced cytoplasmic extensions (compare with Figure 3B). **E.** TEM of hemocyte near middle of a nodule, formed after 15 min of incubation with bacteria, that has retained an ovoid outline and is separated from adjacent cells by extracellular spaces. Arrows point to phagocytic vacuoles, some empty and one containing a partially degraded bacterium (*). **F.** TEM showing elongate, flattened hemocytes along the surface of a nodule after 4 h of incubation. **G.** Scanning electron micrograph showing individual hemocytes attached to the bottom of a petri dish after being incubated with the tripeptide Arg–Gly–Asp (RGD) for 1 h. Hemocytes display blebs (white arrows) on their surfaces, but they have not flattened; they show no filopodia or lamellipodia, and no cell aggregates were observed. Scale bars: A,C = 15 μm; B = 10 μm; D–F = 4 μm; G = 20 μm. es, extracellular spaces; fh, flattened hemocyte; h, hemocyte; lp, lamellipodium; m, mitochondria; n, nucleus

weight over a range in limpet mass from 100 to 500 g. The linear equation describing this relationship based on the 14 measurements was $y = 0.489x + 1.58$ ($F_{[1,12]} = 243.6$, $R^2 = 0.949$, $p < .001$), where y is hemolymph volume and x is mass.

Bacterial cells (*Vibrio fischeri*) were injected into the subesophageal sinus of six limpets. Assuming rapid mixing with the estimated total hemolymph in each limpet, the bacterial dose yielded a final concentration of 10^4 bacteria/ml hemolymph. Bacteria were significantly and rapidly cleared from circulation ($F_{[4,20]} = 815.3$, $p < .001$); the change in bacterial concentration followed an exponential decay model ($w_i = 0.77$), and the number of remaining bacteria decreased significantly at every observation time ≤24 h ($p < .001$; Figure 5B). Although there was variation among individual limpets at early times, the trend was clear and bacteria were undetectable within 48 h. THC varied significantly over time depending on injection treatment ($F_{[8,64]} = 10.3$, $p < .001$; Figure 5C). Merely puncturing the limpets to obtain a small sample of blood for a THC showed a small, nonsignificant increase in hemocyte abundance after 8 h. Total hemocyte counts were significantly different ($p < .001$) between both the bacteria and PBS + NaCl treatments and the puncturing treatment at 1, 4, and 8 h, but not at 24 or 48 h. There was a rapid decline in the THC in the first hour following the injection of bacteria. This reduction was followed by a gradual return to the initial levels by 24 h. At 24 h, several of the limpets had a THC exceeding the initial value, and this continued to 48 h. The six limpets injected with PBS + NaCl showed a similar response: a decline in THC until 4 h after injection, followed by an increase in circulating hemocytes, which often exceeded the initial values by 48 h. However, THCs were significantly lower in the bacteria treatment than in the PBS + NaCl treatment at both 1 h ($p = .004$) and 4 h ($p = .015$) after injection.

3.5 | Morphology of nodules binding to tissues in vivo

SEM images of the ventral surface of the buccal mass, slightly posterior to the site where bacteria were typically injected into limpets, showed a clean surface covered by cells with short apical microvilli (Figure 6A,C). Hemocytes bound to the surfaces of the circulatory system were rarely observed, and if present, they occurred individually and never in aggregates. For comparison, when bacteria were injected into two limpets, the injection needle was glued in place such that it could be found upon dissection, and adjacent tissue was quickly removed and processed for examination using SEM. In these two samples, nodules were commonly found bound to the external surface of the buccal mass (Figure 6B,D); hemocytes displayed lamellipodia and were partially covered by material presumed to be precipitated hemolymph proteins. These observations suggest that nodule formation in vivo creates adhesive cells which may bind to tissues, thereby reducing the circulating level of hemocytes.

4 | DISCUSSION

In this study, we demonstrate that exposure to foreign material, such as bacteria, latex beads, and even the plastic of petri dishes, immediately initiates morphological changes in the hemocytes of *M. crenulata*: hemocytes change from circulating, ovoid cells into adhesive cells that bind to other hemocytes and foreign materials. Hemocytes in the resulting nodules extend cytoplasmic projections and phagocytose foreign particles. Within 4 h of the initiation of nodule formation, hemocytes have become flattened, extracellular spaces have been reduced or eliminated, and nodules appear compact with relatively smooth surfaces. The binding and phagocytosis of foreign particles by hemocytes during nodule formation appears to be an important mechanism by which bacteria are rapidly cleared from circulation (Cueto et al., 2015; Núñez et al., 1994; Pauley et al., 1971; Pauley & Krassner, 1972; van der Knaap et al., 1981). Núñez et al. (1994) provide evidence that a parasitic infection may suppress this immune response. The clearance of bacteria corresponds to a decrease in the number of circulating hemocytes. In vitro cultures of hemocytes also show removal of bacteria from suspension and mimics the in vivo experiments. Our in vivo experiments demonstrated clearance of 65.8% ± 7.6 (mean ± 95% CI) of the bacteria after 4 h and complete elimination of bacteria by 48 h, whereas our in vitro
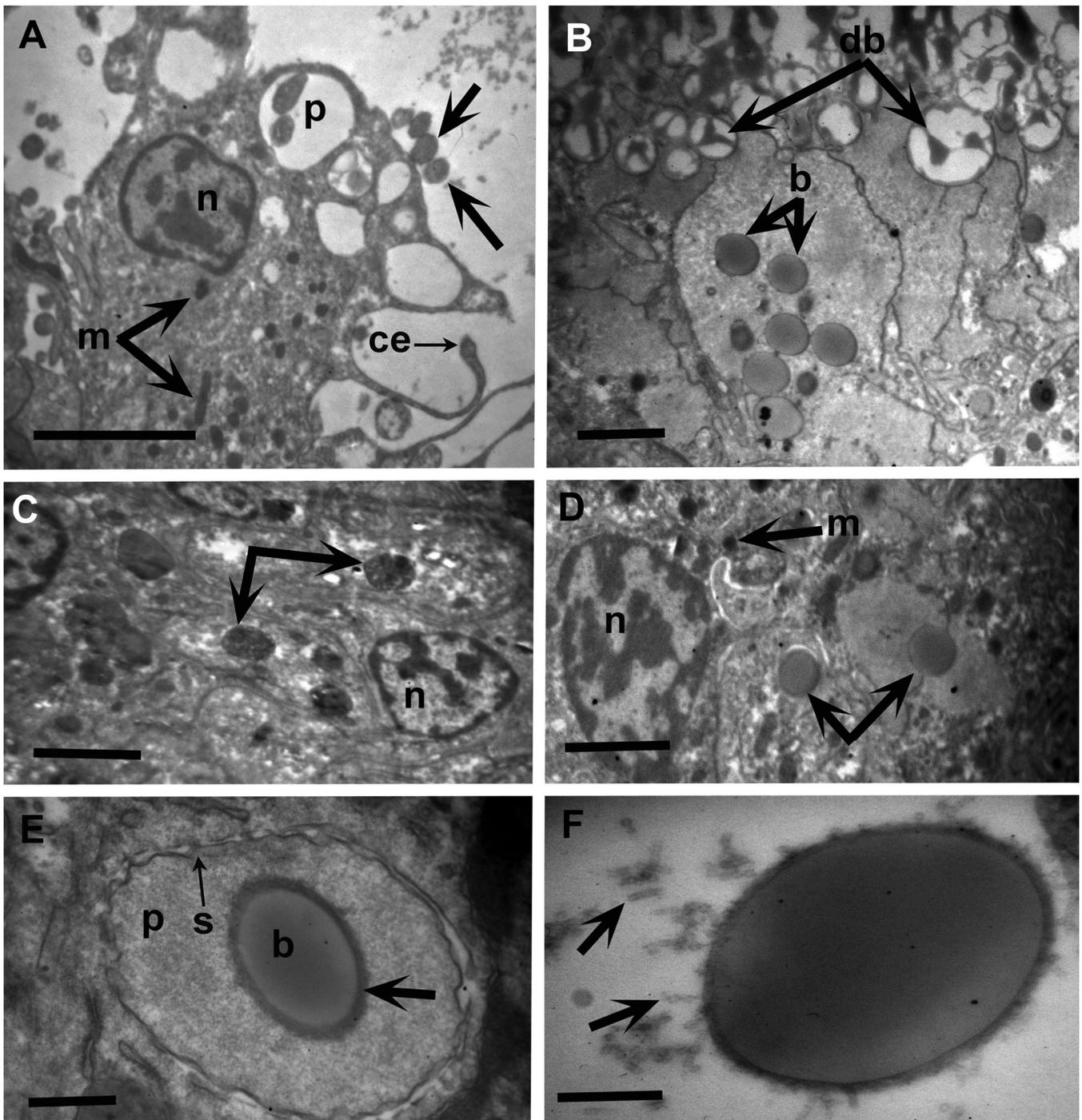
FIGURE 4   Transmission electron micrographs of nodules formed by hemocytes in *Megathura crenulata*. **A.** TEM of one hemocyte on the surface of a 15 min nodule, showing cytoplasmic extensions along with bacteria bound to its surface (arrows) and within a phagocytic vacuole. **B.** TEM of hemocytes along surface of nodule after 15 min of incubation with latex beads, showing numerous collapsed and distorted beads along the surfaced of the nodule and unaltered beads within a phagosome. The latter appear circular and have a homogeneous, moderately electron-dense content. **C.** TEM of elongate and tightly packed hemocytes from the center of a nodule after 1-h incubation. Note the phagocytic vacuoles containing digested bacterial products (arrows). **D.** TEM showing beads (arrows) within hemocytes from the center of a nodule after 1-h incubation. Note that the cells are tightly packed with no intervening spaces. **E.** TEM of a bead within a phagocytic vacuole after 15 min of incubation. Note the moderately electron-dense bead, a denser bounding layer (arrow), and the surrounding, sculpted membrane of the phagosome. **F.** TEM of a bead in the plasma external to a nodule, showing an outer, more electron-dense layer with short cylinders (arrows; ~39-nm diameter), some appearing to be binding to the bead. Scale bars: A,C = 5 µm; B,D = 2 µm; E = 0.5 µm; F = 0.3 µm. b, unaltered bead; ce, cytoplasmic extension; db, distorted bead; m, mitochondria; n, nucleus; p, phagocytic vacuole; s, sculpted membrane of phagosome
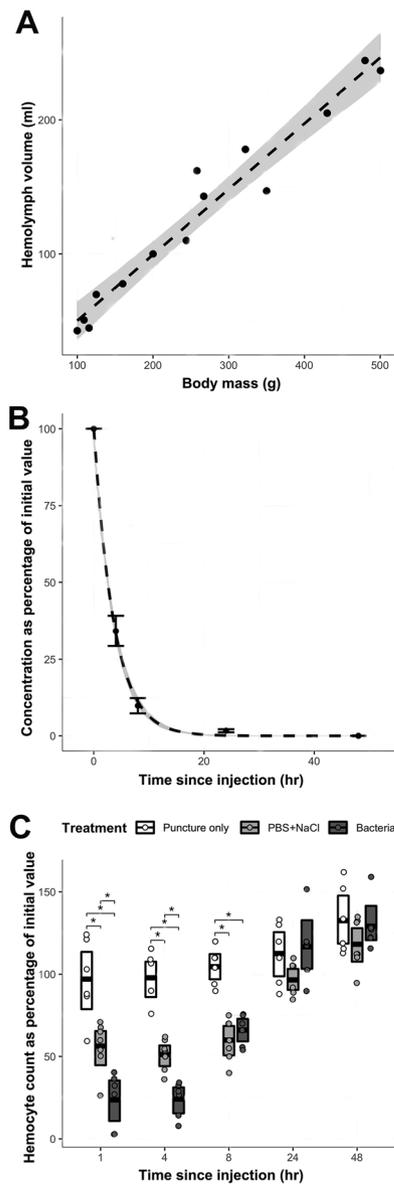
FIGURE 5 Blood volume and hemocyte activation in response to bacteria in the limpet *Megathura crenulata*. **A.** Relationship between body weight and estimated blood volume expressed by the equation $y = 0.489x + 1.58$ ($F_{[1,12]} = 243.6$, $R^2 = 0.949$, $p < .001$, $n = 14$), where y represents blood volume and x represents limpet body mass. Gray ribbon represents 95% confidence intervals of the linear model. **B.** Rate of clearance of the bacteria (*Vibrio fischeri*) from specimens of *M. crenulata* in vivo, expressed as a percentage of bacteria remaining in circulation relative to the estimated bacterial concentration at the time of injection, and monitored over 48 h ($n = 12$). Error bars represent bootstrapped 95% confidence intervals (1000 permutations). Gray ribbon represents 95% confidence intervals of the exponential decay model. **C.** Changes in the total hemocyte count (THC) as a percentage of the initial hemocyte count after in vivo injection of bacterial culture into individuals of *M. crenulata*. Needle puncture alone and injection of PBS + NaCl with no bacteria served as controls. Significant differences ($p < .05$) between treatments at each time are identified by * and brackets. Boxes represent means and bootstrapped 95% confidence intervals (1000 permutations); $n = 6$ for puncture and bacteria treatment; $n = 7$ for PBS + NaCl treatment

experiments showed 83.2% ± 3.5 reductions after 3 h. The in vivo experiments provided a more stable environment for enabling hemocyte–bacteria interactions, but these interactions are easier to observe using the in vitro system. The similarities in the morphological changes in the hemocytes, the efficiency of particle clearance, and the effect on the abundance of individual cells in circulation suggests that the in vitro system can be used to investigate early time points of nodulation in *M. crenulata*. The current study reveals that the effectiveness of nodule formation in eliminating injected foreign particles from circulation in individuals of *M. crenulata* is due to a dynamic hemocyte response and not to antibacterial factors in the plasma because incubation of bacteria in hemocyte-free plasma did not decrease bacterial viability. However, various antibacterial compounds, including lysozyme (Cheng & Gerhart, 1978; Cheng & Mohandas, 1985) and phenoloxidase (Coles & Pipe, 1994; Luna-González et al., 2003), have been reported in other molluscs, and the interaction of these two systems requires further study.

The list of foreign, even abiotic, materials recognized by molluscs has been reviewed in several studies, and this recognition ability shares features with other invertebrates (Lavine & Strand, 2002). The current list suggests that pattern recognition receptors and lectins may be present on the surface of hemocytes in *M. crenulata*. The recognition of abiotic materials which are unlikely to make natural contact with molluscan hemocytes, much less pose threats to infection, is more problematic to explain. Materials such as plastics and metals may not actually be inert, and charges and chemical groups on particles may encourage hemocyte adherence. Lavine and Strand (2002) suggest it is unlikely that cells contain specific receptors for labware such as plastics, and perhaps some receptors are "promiscuous" rather than specific; orphan receptors for which a natural binding ligand is still undiscovered is another possibility (Giguere et al., 1988). The presence of such receptors seems necessary to explain the capability of hemocytes to recognize a wide variety of foreign materials and elicit an immune response to novel materials such as latex beads.

Our observations provide support for two receptors involved with the activation of hemocytes in *M. crenulata*. First, RGD, an amino acid motif recognized by integrins (Kapp et al., 2017; LaFoya et al., 2018) supports the role of integrin-like receptors by blocking hemocytes from becoming adhesive and thereby preventing nodulation in *M. crenulata*. Integrins are membrane proteins that recognize and bind to specific motifs on cell surfaces (Ginsberg, 2014), and these interactions have been well defined in studies on vertebrate white blood cells in which inflammatory chemokines cause integrins to be exposed on cell surfaces leading to their binding and penetration of blood vessels and migration to sites of infection (Begandt et al., 2017). This method of ligand-mediated attraction and adherence has been observed in other molluscs (Canesi et al., 2016). Second, during the incubations that we used to follow phagocytosis in *M. crenulata*, we observed cylinders and particles similar in size and shape to hemocyanin (Figure 4F; see also Gebauer et al., 2002; Harris & Markl, 1999; Martin et al., 2007). These cylinders and particles coated the beads in a way that was similar to hemocyanin-coated beads phagocytosed by cuttlefish hemocytes (Pabic et al., 2014). We speculate that they serve
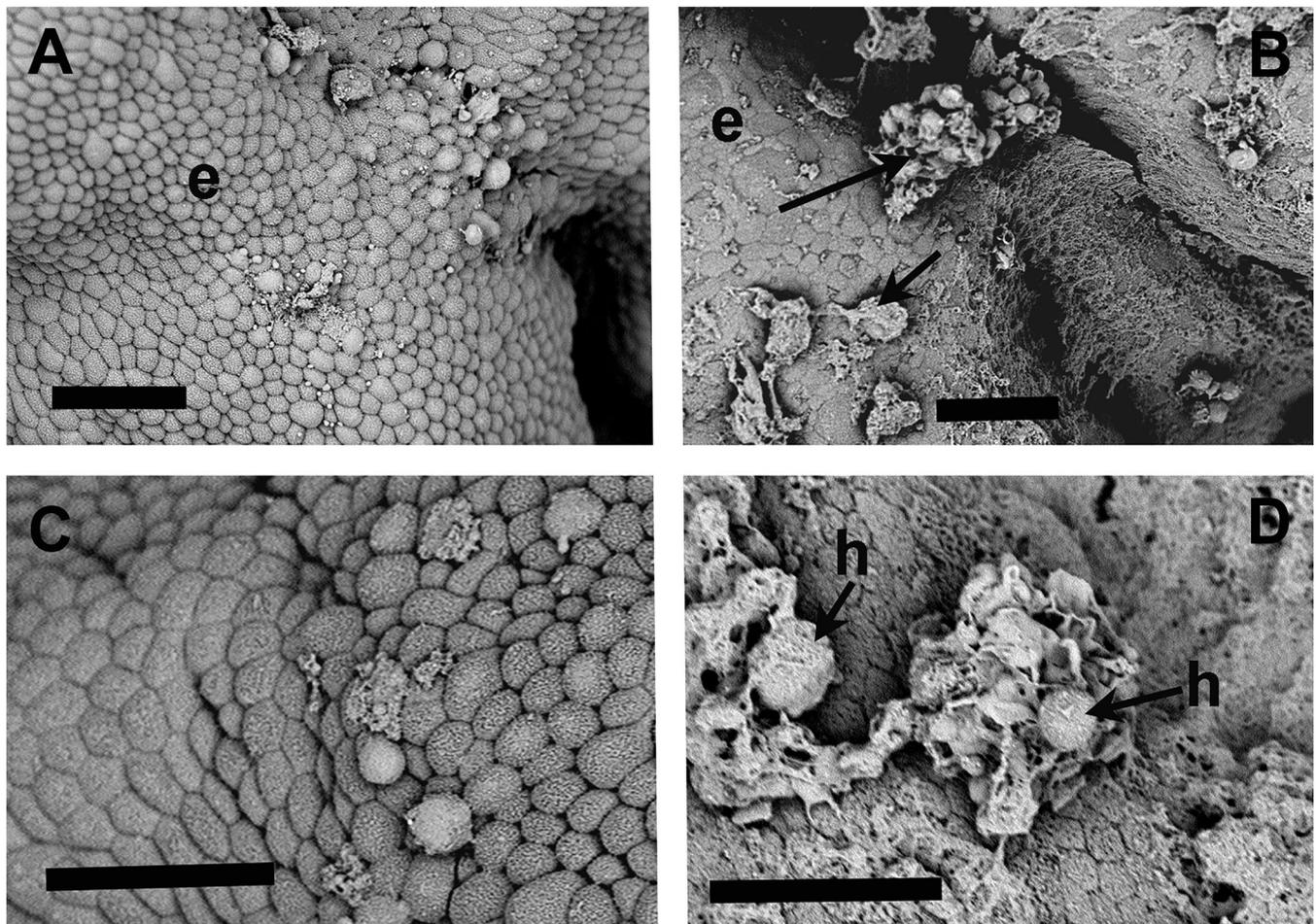
FIGURE 6 Scanning and transmission electron microscopy (SEM) images of the ventral surface of the buccal mass in the limpet *Megathura crenulata*, which suggest that nodules only formed in vivo in animals injected with bacteria (*Vibrio fischeri*). **A,C.** Surface of buccal mass tissue in control limpets, which were only bled (and not exposed to bacterial culture) and then prepared for SEM. The epithelium is clean, with no adhering hemocytes. **B,D.** Surface of the buccal mass tissue, removed from the limpet and processed as above, except that the tissue was prepared 30 min after injection of culture of *V. fischeri*. Note the nodules formed in B are bound to the epithelium. In D, individual hemocytes may be seen with extended lamellipodia, bound to the surface of the epithelia. Scale bars = 300 μm. e, epithelium; h, hemocyte

as an opsonin (i.e., a molecule that binds to foreign materials and enhances their phagocytosis), as described in other studies (Anderson & Good, 1976). KLH has also been shown to activate human monocytic leucocytes (Yasuda & Ushio, 2016). It seems likely that an array of receptors exists that mediate adhesion of limpet hemocytes in addition to these two.

The process of hemocytes becoming adhesive seems to explain the sequestration of foreign particles and the rapid decrease in circulating hemocytes. The rapid decline in THC occurs within 30 min, followed by a gradual increase in the number of circulating cells. Ottaviani (1989) reported a return to initial levels as soon as 60 min, but most reports show an increase beginning after 4 h or longer (Cueto et al., 2015; Dubovskiy et al., 2016; Pauley et al., 1971; Rahmet-Alla & Rowley, 1989; van der Knaap et al., 1981). Injections of bacteria and abiotic particles affect a greater decline in THC than minor pokes through the skin to remove microliter quantities of blood (this study) or the injection of control fluids, such as plasma or sterile seawater (Pauley et al., 1971; van der Knaap et al., 1981). What

differs among species is the proposed site at which hemocytes congregate when lost from circulation. We observed nodules adhering to the epithelia lining parts of the gut bathed in hemolymph. However, our preliminary experiments were performed on a small number of limpets, and the procedure relied on our ability to bleed limpets rapidly enough to reveal the expected site of nodule attachment to tissues without inducing nodule formation by the bleeding methods. Ottaviani and Cossarizza (1990) found evidence in the snail *Planorbarius corneus* for the accumulation of phagocytic cells in the digestive gland and connective tissue of the foot, which does not rule out adhesion to the lining of the circulatory system. Kumazawa and Minei (2001) observed hemocytes in *Clithon retropictum* (MARTENS 1878) migrating into the epithelium of the gut in response to the bacterium *Vibrio parahaemolyticus*. Van der Knaap et al. (1981) highlight a more specific localization, with aggregations primarily in the digestive gland and fixed phagocytes. Research on the apple snail (Cueto et al., 2013, 2015) revealed that nodules form and dilate hemal spaces in the crypts of the kidneys as well as lacunae lining the lung

cavity. It is not clear whether congestion in these narrow vessels requires adhesion only or mechanical congestion in confined hemal spaces.

As nodules form, sequester materials, and are removed from circulation, molluscs then face the challenge of maintaining an effective immune system to prevent further infection until the preferred level of circulating hemocytes is restored. How is the THC is restored? There appear to be three options. There seems to be little support for the first option that the hemocytes within nodules lose their adhesive properties and return into circulation. Nodules in the present in vitro study remained adhered to the petri dish for 48 h and hemocytes never became resuspended in the hemolymph during the observation period; however, the possibility that hemocytes become resuspended in vivo cannot be ruled out. For 48 h, only a tiny percentage (0.7%) of hemocytes took up trypan blue dye or displayed pyknotic nuclei, which suggests that the cells remained healthy. Although we were only able to assess whether individual hemocytes or small nodules (<10 cells) were alive or dead, it seems likely that these cells were the same as those in large nodules because they were morphologically indistinguishable at the LM level. Instead the difference seems to indicate that the great majority of hemocytes bump into other cells and are incorporated into nodules as they settle out of suspension. Cell death at longer incubation times needs to be examined. The second option is that some subset of hemocytes form temporary attachments or reside in tissue sinuses and may be released into circulation when foreign materials are detected. Published reports of fixed hemocytes are based primarily on the examination of preserved materials making it difficult to assess the behavior of these cells. Finally, recent work is beginning to describe hematopoietic organs (Accorsi et al., 2013; Noda & Sato, 1990; Sullivan et al., 1984; and note concern raised by Dos Santos Souza & Andrade, 2012) and the mitotic response of hemocytes to infections. Following the injection of microbes, Salamat and Sullivan (2008) reported an increase in the number of cells dividing within the amebocyte-producing organ of Biomphalaria glabrata, and Rodriguez et al. (2018) reported an increase in dividing hemocytes in the lung and kidneys of Pomacea canaliculata. Studies are needed to determine whether hematopoiesis alone is sufficient to explain the rapid return of THCs to normal levels or higher, or whether other processes are involved as well. Future work should address the fate of nodules sequestering foreign material from the blood as well as continue to explore the factors behind the recognition of foreignness by molluscan hemocytes.

ORCID

Gary G. Martin 🔸 https://orcid.org/0000-0002-5705-1517
Jonathan P. Williams 🔸 https://orcid.org/0000-0002-4829-2474

REFERENCES

Accorsi, A., Bucci, L., Eguileor, M. D., Ottaviani, E., & Malagoli, D. (2013). Comparative analysis of circulating hemocytes of the freshwater snail *Pomacea canaliculata*. *Fish & Shellfish Immunology*, *34*, 1260–1268. https://doi.org/10.1016/j.fsi.2013.02.008

Akaike, H. (1973). Information theory and an extension of the maximum likelihood principle. In B. N. Petran & F. Csaki (Eds.), *Proceedings of the 2nd international symposium on information theory* (pp. 267–281). Akademiai Kiado.

Anderson, R. S., & Good, R. A. (1976). Opsonic involvement in phagocytosis by mollusk hemocytes. *Journal of Invertebrate Pathology*, *27*, 57–64. https://doi.org/10.1016/0022-2011(76)90028-8

Bartoń, K. (2020). MuMIn: Multi-Model Inference. R package version 1.43.17. https://CRAN.R-project.org/package=MuMIn

Begandt, D., Thome, S., Sperandio, M., & Walzog, B. (2017). How neutrophils resist shear stress at blood vessel walls: Molecular mechanisms, subcellular structures, and cell–cell interactions. *Journal of Leukocyte Biology*, *102*, 699–709. https://doi.org/10.1189/jlb.3mr0117-026rr

Burnham, K. P., & Anderson, D. R. (2002). *Model selection and multimodel inference, a practical information-theoretic approach* (2nd ed.). Springer Science + Business Media.

Canesi, L., Grande, C., Pezzati, E., Balbi, T., Vezzulli, L., & Pruzzo, C. (2016). Killing of *vibrio cholerae* and *Escherichia coli* strains carrying D-mannose-sensitive ligands by *Mytilus* hemocytes is promoted by a multifunctional hemolymph serum protein. *Microbial Ecology*, *72*, 759–762. https://doi.org/10.1007/s00248-016-0757-1

Canesi, L., Scarpato, A., Betti, M., Ciacci, C., Pruzzo, C., & Gallo, G. (2002). Bacterial killing by *Mytilus* hemocyte monolayers as a model for investigating the signaling pathways involved in mussel immune defense. *Marine Environmental Research*, *54*, 547–551. https://doi.org/10.1016/s0141-1136(02)00144-7

Chen, J. H., & Bayne, C. J. (1995). Bivalve mollusc hemocyte behaviors: Characterization of hemocyte aggregation and adhesion and their inhibition in the California mussel (*Mytilus californianus*). *The Biological Bulletin*, *188*, 255–266. https://doi.org/10.2307/1542303

Cheng, T. C. (1981). Bivalves. In N. A. Ratcliffe & A. F. Rowley (Eds.), *Invertebrate blood cells* (pp. 233–300). Academic Press.

Cheng, T. C., & Gerhart, P. L. (1978). Aminopeptidase and lysozyme activity levels and serum protein concentrations in *Biomphalaria glabrata* (Mollusca) challenged with bacteria. *Journal of Invertebrate Pathology*, *32*, 297–302. https://doi.org/10.1016/0022-2011(78)90192-1

Cheng, T. C., & Mohandas, A. (1985). Effect of high dosages of bacterial challenge on acid phosphatase release from *Biomphalaria glabrata* hemocytes. *Journal of Invertebrate Pathology*, *45*, 236–241. https://doi.org/10.1016/0022-2011(85)90014-x

Coles, J. A., & Pipe, R. K. (1994). Phenoloxidase activity in the haemolymph and haemocytes of the marine mussel *Mytilus edulis*. *Fish & Shellfish Immunology*, *4*, 337–352. https://doi.org/10.1006/fsim.1994.1030

Cueto, J. A., Rodriguez, C., Vega, I. A., & Castro-Vazquez, A. (2015). Immune defenses of the invasive apple snail *Pomacea canaliculata* (Caenogastropoda, Ampullariidae): Phagocytic hemocytes in the circulation and the kidney. *PLoS ONE*, *10*(4), e0123964. https://doi.org/10.1371/journal.pone.0123964

Cueto, J. A., Vega, I. A., & Castro-Vazquez, A. (2013). Multicellular spheroid formation and evolutionary conserved behaviors of apple snail hemocytes in culture. *Fish & Shellfish Immunology*, *34*, 443–453. https://doi.org/10.1016/j.fsi.2012.11.035

Davids, B. J., & Yoshino, T. P. (1998). Integrin-like RGD-dependent binding mechanism involved in the spreading response of circulating molluscan phagocytes. *Developmental & Comparative Immunology*, *22*, 39–53. https://doi.org/10.1016/s0145-305x(97)00039-6

Dikkeboom, R., Knaap, W. P., Maaskant, J. J., & Jonge, A. J. (1985). Different subpopulations of haemocytes in juvenile, adult and *Trichobilharzia ocellata* infected *Lymnaea stagnalis*: A characterization

using monoclonal antibodies. *Zeitschrift Fur Parasitenkunde Parasitology Research*, 71, 815–819. https://doi.org/10.1007/bf00926806

dos Santos Souza, S., & Andrade, Z. (2012). The significance of the amoebocyte-producing organ in *Biomphalaria glabrata*. *Memórias Do Instituto Oswaldo Cruz*, 107, 598–603. https://doi.org/10.1590/S0074-02762012000500005

Dubovskiy, I., Kryukova, N. A., & Ratcliffe, N. A. (2016). Encapsulation and nodulation in insects. *Invertebrate Survival Journal*, 13, 229–246.

Fenstermaker, R. A., Ciesielski, M. J., Qiu, J., Yang, N., Frank, C. L., Lee, K. P., & Hutson, A. D. (2016). Clinical study of a surviving long peptide vaccine (SurVaxM) in patients with recurrent malignant glioma. *Cancer Immunology, Immunotherapy*, 65, 1339–1352. https://doi.org/10.1007/s00262-016-1890-x

Franchini, A., & Ottaviani, E. (2000). Repair of molluscan tissue injury: Role of PDGF and TGF-β. *Tissue and Cell*, 32, 312–321. https://doi.org/10.1054/tice.2000.0118

Gebauer, W., Harris, J. R., & Markl, J. (2002). Topology of the 10 subunits within the decamer of KLH, the hemocyanin of the marine gastropod *Megathura crenulata*. *Journal of Structural Biology*, 139, 153–159. https://doi.org/10.1016/s1047-8477(02)00591-9

Giguere, V., Yang, N., Segui, P., & Evans, R. M. (1988). Identification of a new class of steroid hormone receptors. *Nature*, 331, 91–94. https://doi.org/10.1038/331091a0

Ginsberg, M. H. (2014). Integrin activation. *BMB Reports*, 47, 655–659. https://doi.org/10.5483/bmbrep.2014.47.12.241

Giron-Perez, M. I. (2010). Relationships between innate immunity in bivalve molluscs and environmental pollution. *Invertebrate Survival Journal*, 7, 149–156.

Giulianini, P. G., Bertolo, F., Battistella, S., & Amirante, G. A. (2003). Ultrastructure of the hemocytes of *Cetonischema aeruginosa* larvae (Coleoptera, Scarabaeidae): Involvement of both granulocytes and oenocytoids in *in vivo* phagocytosis. *Tissue & Cell*, 35, 243–251. https://doi.org/10.1016/S0040-8166(03)00037-5

Gliński, Z., & Jarosz, J. (1997). Molluscan immune defenses. *Archivum Immunologiae et Therapiae Experimentalis*, 45, 149–155.

Gopalakrishnan, S., Thilagam, H., Huang, W., & Wang, K. (2009). Immunomodulation in the marine gastropod *Haliotis diversicolor* exposed to benzy(a)pyrene. *Chemosphere*, 75, 389–397. https://doi.org/10.1016/j.chemosphere.2008.12.027

Greenwell, B. M., & Schubert Kabban, C. M. (2014). Investr: An R package for inverse estimation. *The R Journal*, 6(1), 90–100. http://journal.r-project.org/archive/2014-1/greenwell-kabban.pdf. https://doi.org/10.32614/RJ-2014-009

Hanington, P. C., Forys, M. A., Dragoo, J. W., Zhang, S., Adema, C. M., & Loker, E. S. (2010). Role for a somatically diversified lectin in resistance of an invertebrate to parasite infection. *Proceedings of the National Academy of Sciences*, 107, 21087–21092. https://doi.org/10.1073/pnas.1011242107

Harris, J. R., & Markl, J. (1999). Keyhole limpet hemocyanin (KLH): A biomedical review. *Micron*, 30, 597–623.

Humphries, J. E., & Yoshino, T. P. (2003). Cellular receptors and signal transduction in molluscan hemocytes: Connections with the innate immune system of vertebrates. *Integrative and Comparative Biology*, 43, 305–312. https://doi.org/10.1093/icb/43.2.305

Kapp, T. G., Rechenmacher, F., Neubauer, S., Maltsev, O. V., Cavalcanti-Adam, E. A., Zarka, R., & Kessler, H. (2017). A comprehensive evaluation of the activity and selectivity profile of ligands for RGD-binding Integrins. *Scientific Reports*, 7, 1–13. https://doi.org/10.1038/srep39805

Koutsogiannaki, S., & Kaloyianni, M. (2010). Signaling molecules involved in immune responses in mussels. *Invertebrate Survival Journal*, 7, 11–21.

Kumazawa, N. H., & Minei, A. (2001). Migratory responses of hemocytes to *Vibrio parahaemolyticus* in the alimentary tract of an estuarine neritid gastropod, *Clithon retropictus*. *Journal of Veterinary Medical Science*, 63, 1257–1261. https://doi.org/10.1292/jvms.63.1257

Lafoya, B., Munroe, J., Miyamoto, A., Detweiler, M., Crow, J., Gazdik, T., & Albig, A. (2018). Beyond the matrix: The many non-ECM ligands for integrins. *International Journal of Molecular Sciences*, 19, 449. https://doi.org/10.3390/ijms19020449

Lavine, M. D., & Strand, M. R. (2002). Insect hemocytes and their role in immunity. *Insect Biochemistry and Molecular Biology*, 32, 1295–1309. https://doi.org/10.1016/S0965-1748(02)00092-9

Lenth, R. V. (2021). emmeans: Estimated Marginal Means, aka Least-Squares Means. R package version 1.6.1. https://CRAN.R-project.org/package=emmeans

Loker, E. S. (2010). Gastropod immunobiology. *Advances in Experimental Medicine and Biology Invertebrate Immunity*, 708, 17–43. https://doi.org/10.1007/978-1-4419-8059-5_2

Loker, E. S., Adema, C. M., Zhang, S., & Kepler, T. B. (2004). Invertebrate immune systems - not homogeneous, not simple, not well understood. *Immunological Reviews*, 198, 10–24. https://doi.org/10.1111/j.0105-2896.2004.0117.x

Luna-González, A., Maeda-Martínez, A. N., Vargas-Albores, F., Ascencio-Valle, F., & Robles-Mungaray, M. (2003). Phenoloxidase activity in larval and juvenile homogenates and adult plasma and haemocytes of bivalve molluscs. *Fish & Shellfish Immunology*, 15, 275–282. https://doi.org/10.1016/s1050-4648(02)00165-1

Martin, A. W., Harrison, F. M., Juston, M. J., & Stewart, D. M. (1958). The blood volumes of some representative molluscs. *Journal of Experimental Biology*, 35, 260–279. https://doi.org/10.1242/jeb.35.2.260

Martin, G. G., Bailey, A. K., Cohen, S., Loera, Y., Crooke, A. M., Stamnes, S., & Rose, K. (2018). Morphology and function of the skin epithelium covering the giant keyhole limpet *Megathura crenulata*. *Invertebrate Biology*, 137, 151–170. https://doi.org/10.1111/ivb.12213

Martin, G. G., Bessette, T., Martin, A., Cotero, R., Vumbaco, K., & Oakes, C. (2010). Morphology of epithelial cells lining the digestive tract of the giant keyhole limpet, *Megathura crenulata* (Mollusca: Vetigastropoda). *Journal of Morphology*, 271, 1134–1151. https://doi.org/10.1002/jmor.10862

Martin, G. G., Oakes, C. T., Tousignant, H. R., Crabtree, H., & Yamakawa, R. (2007). Structure and function of haemocytes in two marine gastropods, *Megathura crenulata* and *Aplysia californica*. *Journal of Molluscan Studies*, 73, 355–365. https://doi.org/10.1093/mollus/eym032

Matricon-Gondran, M., & Letocart, M. (1999). Internal defenses of the snail *Biomphalaria glabrata*. *Journal of Invertebrate Pathology*, 74, 224–234. https://doi.org/10.1006/jipa.1999.4876

Mikulski, C. M., Burnett, L., & Burnett, K. (2000). The effects of hypercapnic hypoxia on the survival of shrimp challenged with *Vibrio parahaemolyticus*. *Journal of Shellfish Research*, 19, 301–311.

Miles, D., Roche, H., Martin, M., Perren, T. J., Cameron, D. A., Glaspy, J., & Ibrahim, N. K. (2011). Phase III multicenter clinical trial of the sialyl-TN (STn)-keyhole limpet hemocyanin (KLH) vaccine for metastatic breast cancer. *The Oncologist*, 16, 1092–1100. https://doi.org/10.1634/theoncologist.2010-0307

Morris, R. H., Abbott, D. P., & Haderlie, E. C. (1980). *Intertidal invertebrates of California*. Stanford University Press.

Noda, S., & Sato, A. (1990). Effects of infection with *Angiostrongylus cantonensis* on the circulating haemocyte population and the haematopoietic organ of the host snail M-line *Biomphalaria glabrata*. *Journal of Helminthology*, 64, 239–247. https://doi.org/10.1017/s0022149x00012220

Núñez, P. E., Adema, C. M., & de Jong-Brink, M. (1994). Modulation of the bacterial clearance activity of hemocytes from the fresh-water mollusk, *Lymnaea stagnalis*, by the avian schistosome, *Trichobilharzia ocellata*. *Parasitology*, 109, 299–310. https://doi.org/10.1017/S0031182000078331

Onofri, A. (2020). *The broken bridge between biologists and statisticians: A blog and R package*. Statforbiology. https://www.statforbiology.com

Ottaviani, E. (1989). Haemocytes of the freshwater snail *Viviparus ater* (Gastropoda, Prosobranchia). *Journal of Molluscan Studies*, *55*, 379–382. https://doi.org/10.1093/mollus/55.3.379

Ottaviani, E., & Cossarizza, A. (1990). Immunocytochemical evidence of vertebrate bioactive peptide-like molecules in the immuno cell types of the freshwater snail *Plianorbarius corneus* (L.) (Gastropoda, Pulmonata). *FEBS Letters*, *267*, 250–252. https://doi.org/10.1016/0014-93(90)80937-e

Ottaviani, E., Franchini, A., & Fontanili, P. (1992). The presence of immuno-reactive vertebrate bioactive peptide substances in hemocytes of the freshwater snail *Viviparus ater* (Gastropoda, Prosobranchia). *Cellular and Molecular Neurobiology*, *12*, 455–462. https://doi.org/10.1007/bf00711546

Pabic, C. L., Goux, D., Guillamin, M., Safi, G., Lebel, J., Koueta, N., & Serpentini, A. (2014). Hemocyte morphology and phagocytic activity in the common cuttlefish (*Sepia officinalis*). *Fish & Shellfish Immunology*, *40*, 362–373. https://doi.org/10.1016/j.fsi.2014.07.020

Pauley, G. B., & Krassner, S. M. (1972). Cellular defense reactions to particulate materials in the California Sea hare, *Aplysia californica*. *Journal of Invertebrate Pathology*, *19*, 18–27. https://doi.org/10.1016/0022-2011(72)90183-8

Pauley, G. B., Krassner, S. M., & Chapman, F. A. (1971). Bacterial clearance in the California Sea hare, *Aplysia californica*. *Journal of Invertebrate Pathology*, *18*, 227–239. https://doi.org/10.1016/0022-2011(71)90150-9

Pengsakul, T., Suleiman, Y. A., & Cheng, Z. (2013). Morphological and structural characterization of haemocytes of *Oncomelania hupensis* (Gastropoda: Pomatiopsidae). *The Italian Journal of Zoology*, *80*, 494–502. https://doi.org/10.1080/11250003.2013.825654

Pinheiro J., Bates D., DebRoy S., Sarkar D., & R Core Team. (2021). nlme: Linear and Nonlinear Mixed Effects Models. R package version 3.1–152. https://CRAN.R-project.org/package=nlme

Pyzer, A. R., Avigan, D. E., & Rosenglatt, J. (2014). Clinical trials of dendritic cell-based cancer vaccines in hematologic malignancies. *Human Vaccines & Immunotherapeutics*, *10*, 3215–3131. https://doi.org/10.4161/21645515.2014.982993

R Core Team. (2021). R: A language and environment for statistical computing. R Foundation for Statistical Computing, Vienna, Austria. https://www.R-project.org/

Rahmet-Alla, M., & Rowley, A. F. (1989). Studies on the cellular defense reactions of the Madeira cockroach, *Leucophaea maderae*: Nodule formation in response to injected bacteria. *Journal of Invertebrate Pathology*, *54*, 200–207. https://doi10.1016/0022-2011(89)90029-3

Robohm, R. A. (1984). In vitro phagocytosis by molluscan hemocytes: A survey and critique of methods. In T. C. Cheng (Ed.), *vertebrate blood* (pp. 147–172). Springer. https://doi.org/10.1007/978-1-4684-4766-8_6

Rodriguez, C., Prieto, G. I., Vega, I. A., & Castro-Vazquez, A. (2018). Assessment of the kidney and lung as immune barriers and hematopoietic sites in the invasive apple snail *Pomacea canaliculata*. *PeerJ*, *6*, e5789. https://doi.org/10.7717/peerj.5789

Salamat, Z., & Sullivan, J. T. (2008). *In vitro* mitotic responses of the amebocyte-producing organ of *Biomphalaria glabrata* to extracts of *Schistosoma mansoni*. *Journal of Parasitology*, *94*, 1170–1173. https://doi.org/10.1645/GE-1554.1

Sminia, T. (1972). Structure and function of blood and connective tissue cells of the fresh water pulmonate *Lymnaea stagnalis* studied by electron microscopy and enzyme histochemistry. *Zeitschrift Fur Zellforschung Und Mikroskopische Anatomie*, *130*, 497–526. https://doi.org/10.1007/bf00307004

Sminia, T., Borghart-Reinders, E., & Linde, A. W. (1974). Encapsulation of foreign materials experimentally introduced into the freshwater snail *Lymnaea stagnalis*. *Cell and Tissue Research*, *153*, 307–326. https://doi.org/10.1007/bf00229161

Spurr, A. (1969). A low viscosity epoxy embedding medium for electron microscopy. *Journal of Ultrastructure Research*, *245*, 43–49.

Stober, W. (2015). Trypan blue exclusion test of cell viability. *Current Protocols in Immunology*, *111*, A3.B.1–A3.B.3. https://doi.org/10.1002/0471142735.ima03bs111

Sullivan, J. T., Cheng, T. C., & Howland, K. H. (1984). Mitotic responses of the anterior pericardial wall of *Biomphalaria glabrata* (Molusca) subjected to challenge. *Journal of Invertebrate Pathology*, *44*, 114–116. https://doi.org/10.1645/GE-1554.1

Travers, M., Silva, P. M., Goïc, N. L., Marie, D., Donval, A., Huchette, S., & Paillard, C. (2008). Morphologic, cytometric and functional characterization of abalone (*Haliotis tuberculata*) haemocytes. *Fish & Shellfish Immunology*, *24*, 400–411. https://doi.org/10.1016/j.fsi.2007.10.001

van der Knaap, W. P., Sminia, T., Kroese, F. G., & Dikkeboom, R. (1981). Elimination of bacteria from the circulation of the pond snail *Lymnaea stagnalis*. *Developmental and Comparative Immunology*, *5*, 21–32. https://doi.org/10.1016/s0145-305x(81)80004-3

Voltzow, J. (1994). Gastropoda: Prosobranchia. In R. W. Harrison & A. J. Kohn (Eds.), *Microscopic anatomy of invertebrates. Mollusca* (Vol. 5, pp. 111–252). Wiley-Liss.

Yasuda, K., & Ushio, H. (2016). Keyhole limpet hemocyanin induces innate immunity via SYK and ERK phosphorylation. *EXCLI Journal*, *15*, 474–481. https://doi.org/10.17179/excli2016-488

Yousif, F., Blahser, S., & Lammler, G. (1980). The cellular responses in *Marisa cornuarietis* experimentally infected with *Angiostrongylus cantonensis*. *Zeitschrift Fur Parasitenkunde Parasitology Research*, *62*, 179–190. https://doi.org/10.1007/bf00927863